We are IntechOpen,
the world's leading publisher of Open Access books
Built by scientists, for scientists

6,900
Open access books available

185,000
International authors and editors

200M
Downloads

154
Countries delivered to

Our authors are among the

TOP 1%
most cited scientists

12.2%
Contributors from top 500 universities

CLARIVATE ANALYTICS
BOOK CITATION INDEX
INDEXED

WEB OF SCIENCE™

Selection of our books indexed in the Book Citation Index
in Web of Science™ Core Collection (BKCI)

Interested in publishing with us?
Contact book.department@intechopen.com

Numbers displayed above are based on latest data collected.
For more information visit www.intechopen.com

Frost Heave Deformation Analysis Model for Microheave Filler

Ye Yangsheng, Du Xiaoyan, Zhang Qianli and Chai Jinfei

Abstract

With the rapid development of high-speed railway, high-speed railways pose new requirements on subgrade frost heave deformation control. Microheave in conventional non-frost-heave filler cannot meet the requirements of high-speed railways for high levels of smoothness and stability and threaten high-speed train operation safety. To solve problems of seasonal permafrost region subgrade filler microheave in China, combined laboratory test and theoretical analysis, this research analyzed the physical properties of frost heave influencing factors for microheave filler. The influence of skeleton grain during frost heave formation is revealed. The microheave filler frost heave development mechanism is investigated. On this basis, based on the principle of minimum energy, a frost heave calculation formula for microheave filler is deduced, and a frost heave deformation analysis model for microheave filler is created. In addition, the effectiveness of the model is demonstrated in an indoor test. This study provides a theoretical reference for controlling the frost heaving deformation of railway subgrade.

Keywords: high-speed railway subgrade, microheave filler, frost heave influencing factor, frost heave development mechanism, frost heave analysis model

1. Introduction

China now has the world's longest high-speed railway operation mileage, fastest operational speed and largest scale of projects under construction. By the end of 2016, the high-speed railway operational mileage had reached 2.2×10^4 km, which was the largest in the world. Compared with normal speed railways, the major features of high-speed railways are that they are fast, comfortable and safe. For ballasted track, high-speed railway subgrade settlement should not exceed 5 or 3 cm in transition segments. For ballastless track high-speed railway subgrades, the ideal goal in actual projects is zero settlement, in particular for deformation-sensitive sections such as transit segments, for which settlement is controlled to be under 5 mm and to not exceed 1/1000 at corners. To achieve the above goal, track structure smoothness and stability should be guaranteed, which is reliant on providing track structures with subgrade structures of high strength, high rigidity, uniform longitudinal variation, high stability and durability. Currently, in northeast China, the Harbin-Dalian, Panjin-Yingkou, Harbin-Qiqihar, Shenyang-Dandong and Jilin-Hunchun high-speed railways span seasonal permafrost regions. Compared with high-speed railways in non-frost regions, for high-speed railways in permafrost regions, subgrade filler frost heave induces uneven settlement, which

has become a critical issue [1]. In northern China, all railway subgrades have developed various levels of frost heave, which directly threatens travelling safety [2].

In China, both existing high-speed trains and those under construction follow the guidelines in the *Code for Design of Special Subgrade of Railway* (TB10035-2006) regarding filler selection and the design of scattered row impermeable and anti-frost-heave structures. That is, the standard for filler frost heave control is 1%. However, on high-speed railway subgrades in Northeast China, the maximum depth of frost reaches 3 m. According to this standard, subgrade frost heave deformation cannot meet the requirement for ballastless track deformation control. In addition, in the *Code for Design of Special Railway Subgrades*, the seasonal frozen soil frost heave grading object is natural frozen soil, not manually compacted subgrade filler. Therefore, the microheave deformation mechanism for subgrade filler should be investigated, and a microheave deformation analysis model should be created to provide a theoretical basis for specification development and engineering design.

Currently, subgrade seasonal frost heave problems worldwide are investigated via experiments and theoretical models. In an experimentally based investigation, Askar and Zhanbolat investigated the effects of freeze-thaw cycles on a high-speed highway subgrade; a frost heave test was performed using field soil samples to identify frost heave and frost heave pressure in regional soil samples and frost heave depth under different conditions. They suggested that frost heave could be effectively reduced by replacing frost heave sensitive soil with coarse grained soil and deploying a drainage system [3].

Konrad suggested that it was inadequate to determine if subgrade filler had an anti-frost property by grain grading alone; the frost heave properties of fine grains should also be considered [4]. In addition, the frost heave sensitivities of subgrade fillers with superior grading increase linearly with fine grain content and active mineral content [5]. Bilodeau et al. investigated the effects of grain grading and fine grain properties on frost heave sensitivity and found that when fine grain content was low, fine grain mineral composition and grading had greater impacts on frost heave sensitivity. In addition, fine grains with different uniformity coefficients resulted in different frost heave levels [6]. Uthus et al. suggested that the main factors that influenced frost heave were water and fine grains (active minerals). Among these factors, water had greater impacts on frost heave than the material elastic modulus [7].

Wang et al. suggested that frost heave sensitivity and strength of coarse grained soil were affected by fine grain content. Frost heave tests and triaxial tests showed that when the fine grain soil content was 5%, coarse grained soil had weak frost heave property but high shear strength [8]. Bilodeau et al. investigated the relation between freeze-thaw cycle and long-term compression-induced permanent displacement in subgrade coarse grained materials. The results showed that pressure had a greater influence in a saturated soil sample that had not undergone freeze-thaw cycling. In addition, freeze-thaw cycles had a significant influence [9]. Guo et al. performed a frost heave test in a closed system with various levels of water content and compactness as well as in an open system, investigated the Lanzhou-Xinjiang railway subgrade soil frost heave characteristics and reached a conclusion that due to water content replenishment, the frost heave rate in the open system significantly exceeded that in the closed system [10].

In a model-based investigation, Sheng et al. undertook a model test and discovered that train cycle load increased subgrade soil pore hydro-pressure; under the pump suction effect, water level was observed to rise to the frost heave layer, which resulted in continuous frost heave in a high-speed railway subgrade [11]. Abdalla et al. making reasonable assumptions, extended a porosity function model from a

frost heave forecast to a freeze-thaw cycle simulation [12]. Zhang and Michalowski introduced a THM (thermal-hydro-mechanical) model for frost heave sensitive soils such as viscous soils to describe temperature, hydraulic pressure and force field changes induced by freeze-thaw cycling and subsequent physical phenomena such as expansion and settlement; they also provided a numerical simulation for the one-dimensional problem [13]. Bronfenbrener described heat and matter transfer in a fine grain porous medium with frost heave during a phase transition and provided a model for the problem with a movement boundary condition. Comparison with test data proved that within a certain level of precision, the model was viable for frost heave estimation [14]. Yin created a seasonal permafrost region, subgrade soil, multi-factor, frost heave rate forecast model via field measurements and theoretical analysis and applied it to a project [15].

In this paper, based on a field survey in a permafrost region and high-speed railway subgrade filler and frost heave characteristics, the concept of subgrade microheave filler is proposed. A frost heave calculation formula for a microheave filler in closed systems is deduced via an indoor test and theoretical analysis. A frost heave deformation analysis model for microheave filler is created, and its effectiveness is proven.

2. Experimental study on microheave filler frost heave influencing factors

Upon conducting an experimental study, Wang et al. suggested that there were three categories of railway subgrade filler: over coarse grained soils, coarse grained soils and fine grain soils [16]. In this paper, the large amounts of coarse grained soil filler in high-speed railway subgrades in the seasonal permafrost region of China are called microheave filler.

The bed filler used in high-speed railway subgrades in the permafrost regions of China is arranged as follows. A normal embankment bed surface is filled with a layer of 55-cm grading gravel, below which are 5 cm of thick coarse sand and 2.1 m of thick soil in two groups, A and B. In the frozen depth range, the embankment bed is filled with non-frost-heave soil in groups A and B, and soils in groups A, B and C exist below the beds. The top 1.0 m of the embankment bed floor is filled with non-frost-heave filler in groups A and B. Based on the distribution of filler along the line, the lower sections have filler in groups A and B. Low embankment bed surfaces are filled with grading gravel. Non-frost-heave filler in groups A and B is used in the range of the upper meter of bed floors. The lower sections are filled with filler in groups A and B. In the bed floor lower sections, the grading gravel layer water content is 3.2–5.9%, and the fine grain content is 3.2–10.7%. In lower sections, the non-frost-heave soil filler water content generally is 3.7–9.2%, and the fine grain content is 0.4–9.3%. In seasonal permafrost regions, the entire beds are excavated and replaced. The bed surfaces are filled with grading gravel, the upper 1 m of the bed floors are filled with non-frost-heave filler in groups A and B, and the lower sections are filled with filler in groups A and B. The grading gravel layer water contents are 2.2–3.2%, the fine grain contents are 8.0–15.1%, the water contents in the lower section non-frost-heave soil filler are generally 3.7–9.2%, and the fine grain contents are 10.9–16.9%.

Coarse grained soil frost heave tests and analysis proved that the factors that influence major coarse grained soil frost heave include the soil property, water content, temperature and load [17]. To investigate the characteristics of high-speed railway subgrade filler frost heave in permafrost regions, in this chapter, typical permafrost region subgrade soil samples were selected to perform soil property tests

for filler covering water content, liquid plastic limit and grain analysis. On this basis, the effects of various factors on filler frost heave were analyzed to obtain rules regarding the influence of soil fine grain content, compactness, water content, permeability and coarse grain pore filling by fine grains on the properties of coarse grained soil frost heave. It is worth noting that the test reported in this section was based on the conventional liquid and plastic limit combined determination method. In the test, fine grain soil liquid limit water and plastic limit water contents were measured to calculate the soil plasticity index and liquid index, which were used as a basis to evaluate the properties of filler soils. A standard screening test was employed to calculate the relative content of each grain group and to determine soil grain composition. In addition, for subgrades, compactness is not only a control index that ensures subgrade filling quality but also a major factor that affects the properties of filler frost heave. Under identical conditions, as compactness increases, fine grain soil frost heave increases initially and then decreases.

3. Microheave filler frost heave test

3.1 Test apparatus

The frost heave test apparatus consisted of a specimen box, an incubator, a temperature control system, a temperature monitoring system, a deformation monitoring system, a pressure loading system and a water supply system, as shown in **Figure 1**. The specimen box had a diameter of 15 cm and a height of 15 cm.
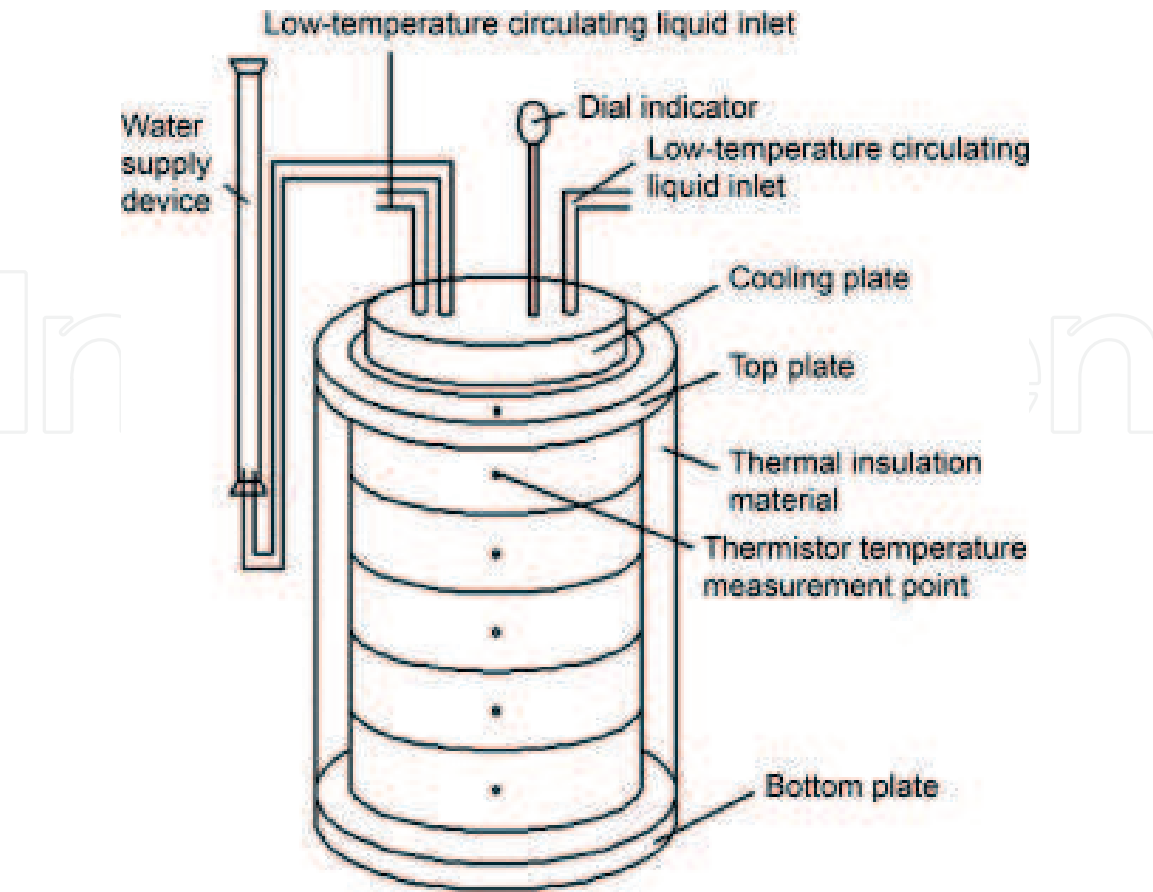
Figure 1.
Frost heave test apparatus.

3.2 Test method

Proper amounts of dry soil samples were mixed with water to produce the required water contents. The soil samples were separated into layers of predefined compactness (5 layers, each with thicknesses of 3 cm) and placed in the specimen box. The specimen box with a sample was placed in the incubator. Thermistor thermometers were deployed on the specimen top plate, bottom plate and side. The specimen box was wrapped in 5 cm of thick plastic foam for heat insulation. The top plate and bottom plate temperatures were controlled using two high precision low temperature circulation cooling systems. A dial indicator was installed on the top plate to monitor specimen deformation. Finally, the temperatures for the specimens were collected automatically via the data collector. The testing was performed in a closed environment. The unidirectional freezing method was applied [18], the duration of the freezing process for each specimen was 72 h, and the direction of freezing was from top to bottom. At the beginning of the tests, the soil column temperature was stabilized at approximately 1°C and maintained for 6 h. The bottom plate temperature was then maintained at 1°C. At 0.5 h, the top plate temperature was decreased to −15°C, and the soil samples were frozen rapidly from the top surface. The top plate temperature was increased to −2°C, and top plate temperature was then decreased by a certain amount per hour. At the conclusion of each test, the soil samples were separated into layers in the low temperature incubator, and the water contents were measured.

3.3 Test items

Test filler was obtained from the subgrade filling soil of a high-speed railway in Northeast China. The grades are listed in **Table 1**. The filler plastic limit ω_p was 19.2%, and the optimal water content ω_0 was 13.2%.

To investigate the effects of factors such as water content, filler and external load on microheave filler frost heave for this paper, a frost heave experimental study was conducted to investigate the following aspects.

1. Effects of filler plastic limit and optimal water content on microheave filler frost heave.

Proper amounts of dry filler were mixed with various amounts of water to produce 30 groups of ω specimens with various levels of initial water content. The initial water content values of the 30 groups of specimens are listed in **Table 2**. The

Grain size range (mm)	content (%)
31.5–45.0	20
22.4–31.5	10
7.1–22.4	25
1.7–7.1	20
0.5–1.7	10
0.1–0.5	9
0.075–0.1	3
<0.075	3

Table 1.
Test filler grades.

Specimen	Initial water content ω(%)
1	12.3
2	14.5
3	15.1
4	15.5
5	15.9
6	16.0
7	16.5
8	18.0
9	18.5
10	18.8
11	19.0
12	19.6
13	20.0
14	20.5
15	21.3
16	13.3
17	14.3
18	14.4
19	14.7
20	15.5
21	15.6
22	15.8
23	16.2
24	16.3
25	17.5
26	17.8
27	18.0
28	19.1
29	19.4
30	21.7

Table 2.
Specimen initial water contents.

first 15 groups of specimens were used to investigate the effects of filler plastic limit on the microheave filler frost heave property, and the next 15 groups of specimens were used to investigate the effects of filler optimal water content on the microheave filler frost heave property. The required amounts of the specimens were calculated based on a compactness of 0.95. The specimens were then compacted in the specimen box for frost heave testing.

2. Effects of volumetric water content on microheave filler frost heave

Proper amounts of dry filler were mixed with various amounts of water to produce 15 groups of ω_V specimens with various levels of initial water content. The initial water content values of the 15 groups of specimens are listed in **Table 3**. The

required amounts of the specimens were calculated based on a compactness of 0.95. The specimens were then compacted in the specimen box for frost heave testing.

3. Effects of filler content and filling rate on microheave filler frost heave

To prepare specimens with the required filler contents, proper amounts of dry filler were mixed with the required filler. In addition, the specimen's filler volume fill rate s was calculated via the following formula.

$$ s = \frac{1-V_1}{V_2} \times 100\% \tag{1} $$

where $V_1 = \frac{M_1}{\gamma_1}$, $V_2 = \frac{M_2}{\gamma_2}$.

V_1 is the filler skeleton grain volume fraction, V_2 is the filler volume fraction, M_1 is the skeleton grain mass for a unit specimen volume, γ_1 is the skeleton grain dry density for the corresponding soil sample compactness, M_2 is the filler mass for a unit specimen volume, and γ_2 is the filler dry density for the corresponding soil sample compactness.

In this test, 15 groups of specimens were prepared. The specimen filler contents and filler filling rates are listed in **Table 4**. In the test, fillers with different contents were used to ensure that the filler skeleton component was proportionally adjusted under the premise that the total mass of filler remained unchanged. All the specimens used in the frost heave test had 15% water content and compactness values of 0.95.

4. Effects of filler frost heave on microheave filler frost heave.

Filler frost heave and pure filler frost heave tests were performed for the 15 groups of filler content specimens prepared in (3) under test conditions of 15% water content and 0.95 compactness [19].

specimen	volumetric water content ωV(%)
1	5.83
2	7.02
3	8.30
4	9.60
5	11.07
6	11.34
7	11.85
8	13.17
9	14.48
10	15.27
11	15.80
12	16.04
13	16.57
14	17.49
15	18.21

Table 3.
Specimen volumetric water contents.

Specimen	Filler content (%)	Filler filling rate (%)
1	1.0	0.056
2	2.0	0.118
3	2.5	0.198
4	2.8	0.272
5	3.0	0.316
6	3.2	0.334
7	5.0	0.363
8	5.5	0.381
9	6.0	0.445
10	9.0	0.465
11	11.0	0.529
12	16.0	0.532
13	18.0	0.606
14	40.0	0.859
15	45.0	0.928

Table 4.
Specimen filler content and filler filling rate.

Figure 2.
Loading apparatus used for the frost heave test.

5. Effects of overlying load on microheave filler frost heave.

A specimen with a 10% filler content was prepared for the frost heave test under test conditions in which the initial water content was 15% and the overlying loads were 5, 10, 20, 30, 40, 55, 65 and 80 kPa. **Figure 2** shows the loading apparatus used in the frost heave test.

4. Analysis of test results

The microheave filler frost heave rate η was calculated via the following formula:

$$\eta = \frac{\Delta h}{H_f} \times 100\% \tag{2}$$

where Δh is the overall specimen frost heave in mm, and H_f is the frozen depth (excluding frost heave) in mm.

4.1 Effects of water content on microheave filler frost heave

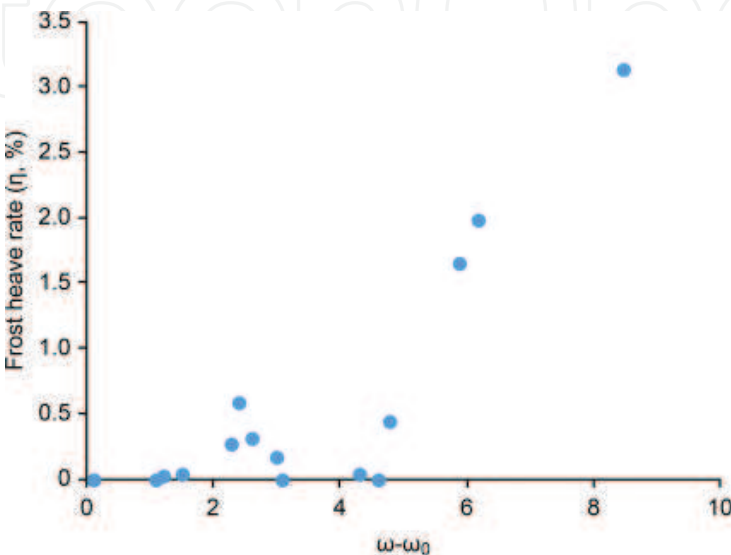1. Relation between filler plastic limit, optimal water content and microheave filler frost heave.

Figure 3 shows the relation between ω-ω_p (difference between the filler initial water content ω and filler plastic limit water content ω_p) and filler frost heave rate η. **Figure 4** shows the relation between ω-ω_0 (difference between the filler initial water content ω and filler optimal water content ω_0) and filler frost heave rate η.

Figures 3 and **4** show that for filler water contents of $\omega \leq \omega_p + 2$ or $\omega \leq \omega_o + 4.6$, the frost heave rate $\eta < 1\%$. However, as the water content increased further, the filler frost heave rate increased significantly.
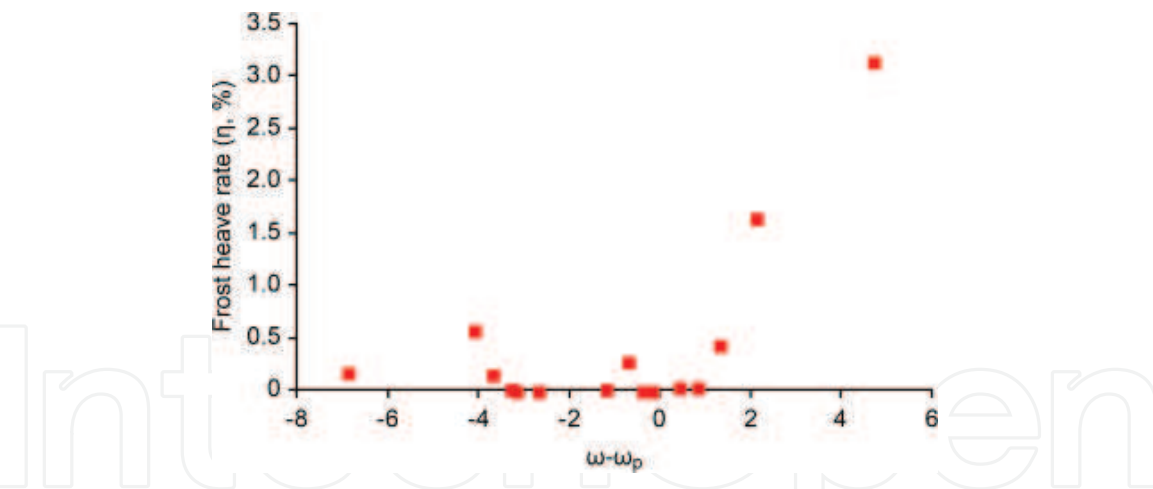
1. Relation between microheave filler volumetric water content and frost heave rate.

Figure 5 shows the relation between the filler volumetric water content ω_v and filler frost heave rate η.

Figure 5 shows that when $\omega_v \leq 13\%$, the filler frost heave rate was insensitive to increases in the volumetric water content, and when $\omega_v > 13\%$, filler frost heave increased significantly with increasing volumetric water content.

Figure 3.
Relation between the filler plastic limit and filler frost heave.

Figure 4.
Relation between the filler optimal water content and filler frost heave.
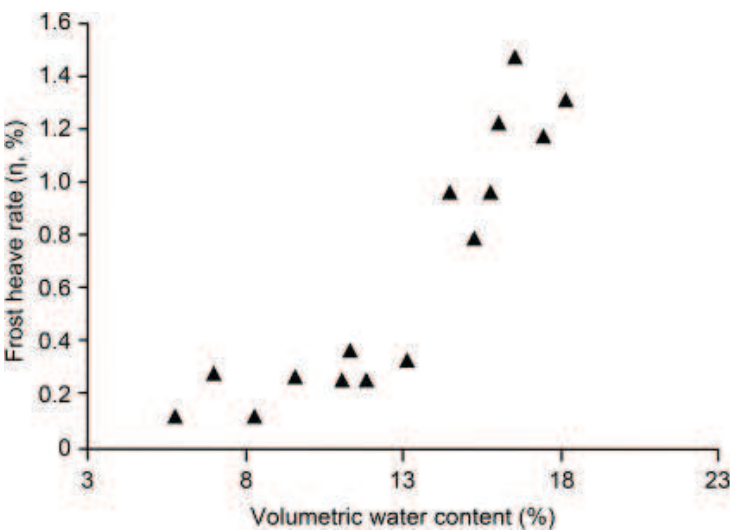
Figure 5.
Relation between the filler volumetric water content and filler frost heave rate.

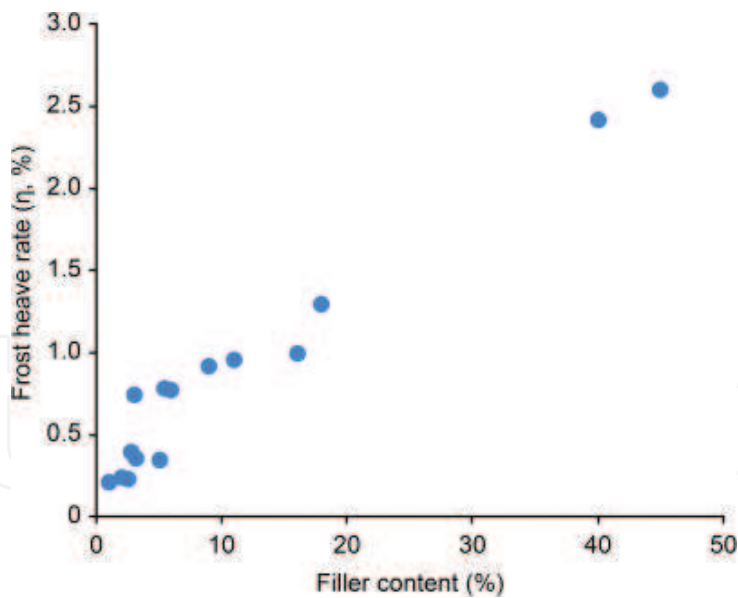## 4.2 Effects of filler on microheave filler frost heave

1. Relation between filler content, filling rate and microheave filler frost heave.

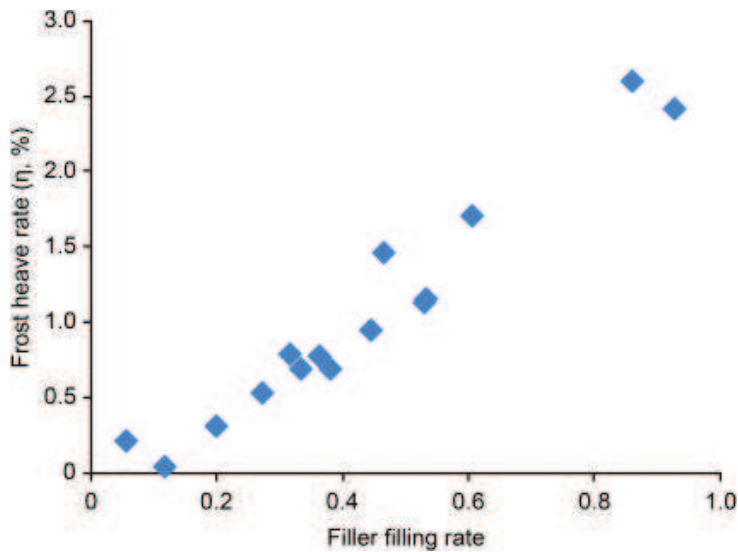**Figure 6** shows the microheave filler frost heave rates for different filler contents.

Figure 6 shows that filler frost heave increased gradually with filler content. When the filler content was under 3%, the frost heave rate was approximately 0.2%, when the filler content was under 15%, the frost heave rate was under 1.0%, and when the filler content exceeded 15%, the filler frost heave sensitivity increased significantly with filler content.

Figure 7 shows the microheave filler frost heave rates for different filler filling rates.

Figure 7 shows that for filler filling rates below 0.18, the filler frost heave rates were under 0.2%, and when the filler filling rates were under 0.25, the filler frost heave rates were under 0.5%; filler frost heave was insensitive to increases in filler content. For filling rates exceeding 0.25, the filler frost heave rates increased significantly with the filling rate, and frost heave became sensitive. For the filling rates were under 0.37, the frost heave rates were under 1.0%.

Figure 6.
Microheave filler frost heave rate for different filler contents.

Figure 7.
Microheave filler frost heave rate for different filler filling rate.
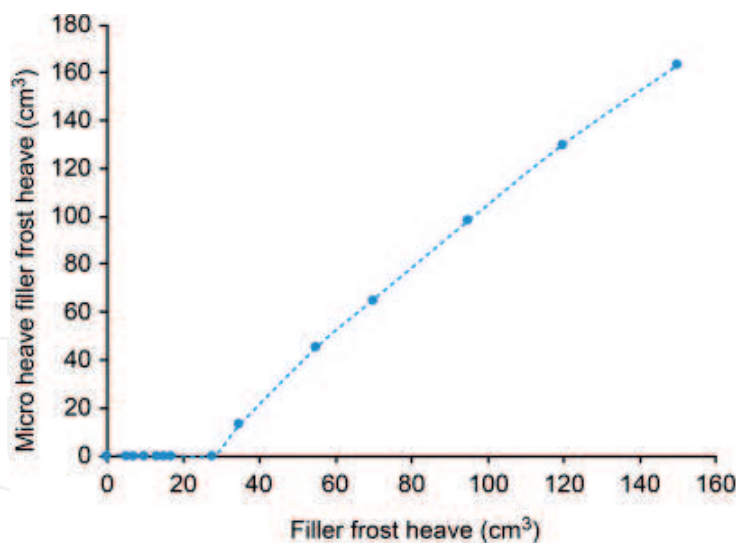
2. Relation between filler frost heave and microheave filler frost heave.

Based on the test results, the relation between specimen filler frost heave and microheave filler frost heave for each group is shown in **Figure 8**.

Figure 8 shows that when filler frost heave was below 25 cm³, the microheave filler exhibited no frost heave. Under this condition, filler frost heave filled pores, and there was no macroscopic filler frost heave. When filler frost heave exceeded 25 cm³, macroscopic frost heave in the microheave filler began and increased significantly with filler frost heave.

4.3 Relation between overlying load and microheave filler frost heave

Overlying loads affect microheave filler frost heave properties in two ways: the freezing point drops with increasing external load, and overlying loads result in

Figure 8.
Filler frost heave versus microheave filler frost heave.
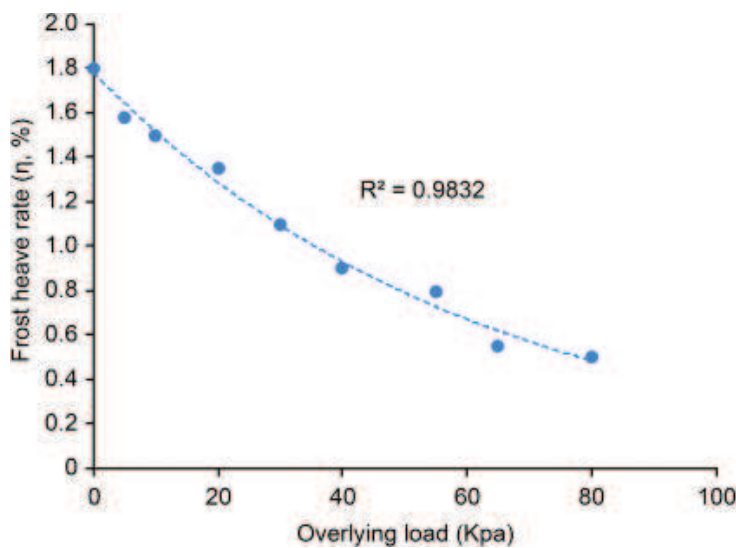
Figure 9.
Relation between frost heave rate and overlying load.

redistributions of filler water content [20]. **Figure 9** shows the microheave filler frost heave rates under different overlying loads.

Figure 9 shows that overlying load and the microheave filler frost heave rate were exponential related. The microheave filler frost heave rate decreased gradually with increasing overlying load.

The indoor test described above provided data for a qualitative analysis of microheave filler frost heave rules. To further investigate frost heave deformation, theoretical analysis and microheave filler frost heave model creation are required.

5. Microheave filler frost heave model

5.1 Microheave filler complete filling analysis

When a microheave filler specimen develops frost heave, the coarse grains do not develop frost heave and act as rigid bodies. By comparison, fine grains develop frost heave at low temperatures. Fine grain component volumes consist of soil grain

and water content volumes. When fine grains develop frost heave, some water content escapes.

In this section, a simulation embodying the direct expansion of filler grains under natural conditions is examined to study filler grain expansion due to water adsorption. To investigate the complete filling of microheave filler, the mixed material specimen model was simplified. The model was assumed to consist of coarse skeletons, filler grains and pores, as shown in **Figures 10** and **11**.

Filler and residual pores constituted the mixed material skeleton pores. Among them, filler fills the skeleton pores, expands at low temperature, and, under the side constraint condition, fills the residual pores first. When the residual pores are filled, the expansion is represented as a mixed material specimen macroscopic expansion.

$$\Delta V_{mixed\ material} = \Delta V_{filler} - \Delta V_{skeleton\ pore} \tag{3}$$

If α represents the filler expansion rate, θ represents the filler content, ρ_{mixed} represents the mixed material compactness, and $G_{skeleton}$ represents the skeleton grain ratio, then

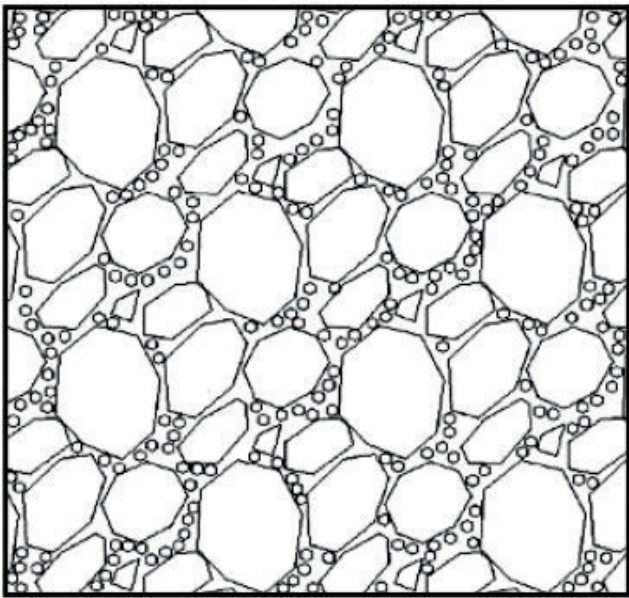$$\Delta V_{skeleton\ pore} = \Delta V_{residual\ pore} \tag{4}$$

From formula (4) and $\Delta V_{filler} = V_{filler}\alpha$,

$$\Delta V_{mixed\ material} = \Delta V_{filler} - \Delta V_{residual\ pore} = \frac{m_{filler}}{\rho_{filler}}(1+\alpha) + \left(\frac{m_{skeleton}}{\rho_{skeleton}}\right) - V_{mixed\ material} \tag{5}$$
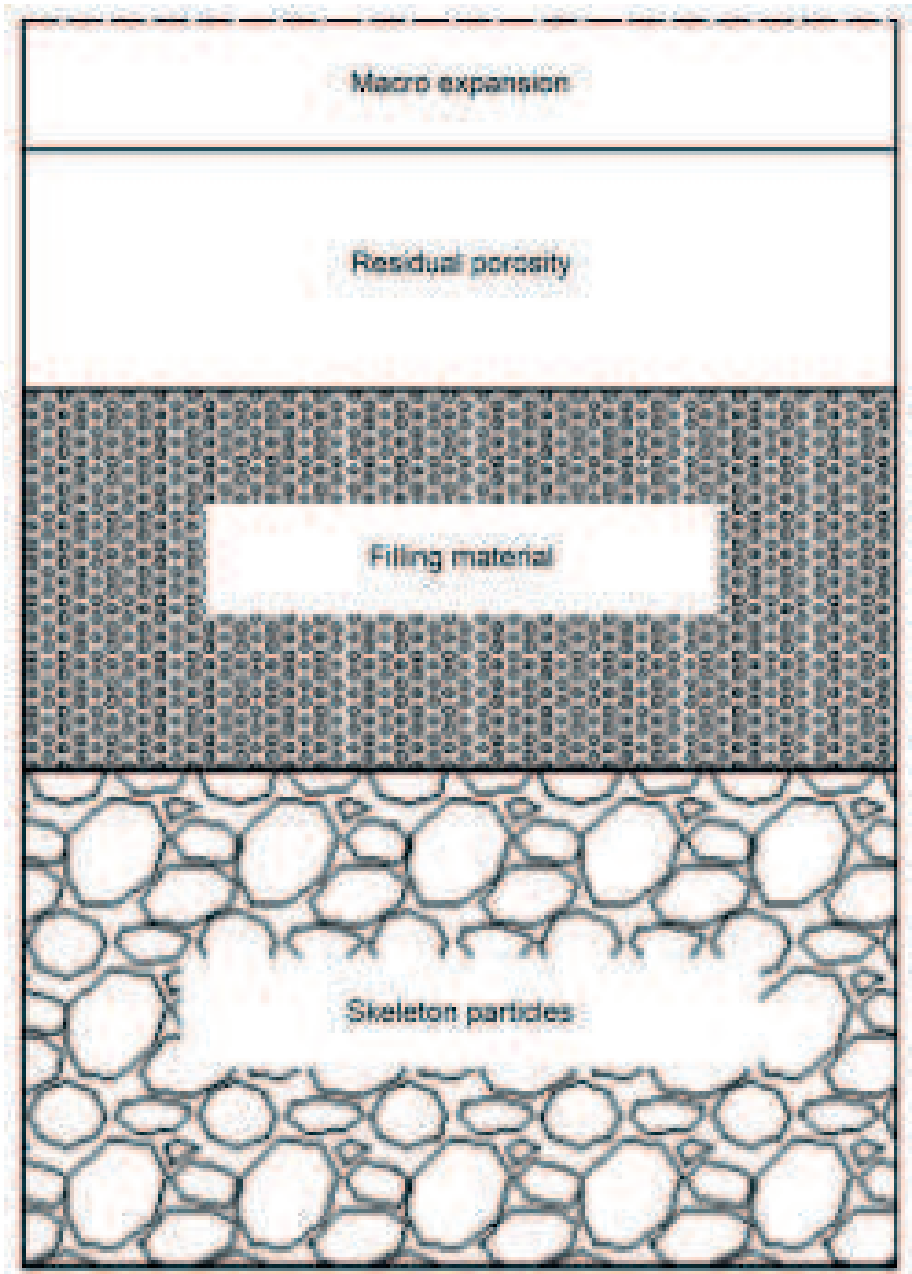
Because

$$m_{filler} = \frac{\theta}{(1-\theta)}m_{skeleton} \tag{6}$$

based on the macroscopic volume expansion rate,

Figure 10.
Mixed material.

Figure 11.
Composition of the mixed material.

$$\eta_{mixed\ material} = \frac{\frac{\Delta V_{mixed\ material}}{\pi R^2}}{\frac{V_{mixed\ material}}{\pi R^2}} = \frac{\Delta V_{mixed\ material}}{V_{mixed\ material}} \tag{7}$$

$$\eta_{filler} = \alpha \tag{8}$$

From formulas (7) and (8),

$$\eta_{mixed\ material} = m_{mixed\ material} \left[\frac{\frac{\theta}{(1-\theta)}(1+\alpha)}{\rho_{filler}} + \frac{1}{\rho_{skeleton}} \right] / V_{mixed\ material} - 1 \tag{9}$$

Because

$$\rho_{mixed} = \frac{m_{skeleton} + m_{mixed\ material}}{V_{mixed\ material}} \tag{10}$$

Based on formulas (6) and (10),

$$m_{skeleton} = \rho(1-\theta)V_{mixed\ material} \tag{11}$$

Combining formulas (9) and (11),

$$\eta_{mixed\ material} = m_{mixed\ material} \left[\frac{\frac{\theta}{(1-\theta)}(1+\alpha)}{\rho_{filler}} + \frac{1}{\rho_{skeleton}} \right] / V_{mixed\ material} - 1$$

$$= \rho_{mixed}(1-\theta) \left[\frac{\frac{\theta}{(1-\theta)}(1+\alpha)}{\rho_{filler}} + \frac{1}{\rho_{skeleton}} \right] - 1 \tag{12}$$

Because the skeleton grain ratio is $G_{skeleton} = \rho_{skeleton}/\rho_w$,
from formula (12),

$$\eta_{mixed\ material} = \rho_{mixed}(1-\theta) \left[\frac{\frac{\theta}{(1-\theta)}(1+\alpha)}{\rho_{filler}} + \frac{1}{G_{skeleton}\rho_w} \right] - 1 \tag{13}$$

Based on the definition of a mixed material skeleton pore, $e = V_{residual\ pore}/V_S$,

$$\rho_{mixed} = \frac{m_{skeleton} + m_{mixed\ material}}{V_{skeleton} + V_{mixed\ material} + V_{residual\ pore}} = \frac{m_{skeleton} + m_{mixed\ material}}{(1+e)(V_{skeleton} + V_{mixed\ material})} \tag{14}$$

and employing the skeleton grain ratio,

$$\rho_{filler} = \frac{\theta}{\frac{1}{(1+e)\rho_{mixed}} - \frac{(1-\theta)}{(G_{skeleton}\rho_w)}} \tag{15}$$

Based on the definition of the porosity ratio,

$$e = \frac{d_s\rho_w(1+0.001w)}{\rho} - 1 = \frac{d_s\rho_w(1+0.001w)}{\rho_{mixed}} - 1 \tag{16}$$

Based on formulas (15) and (16),

$$\rho_{filler} = \frac{\theta}{\frac{1}{(1+e)\rho_{mixed}} - \frac{(1-\theta)}{(G_{skeleton}\rho_w)}} = \frac{\theta}{\frac{1}{d_s\rho_w(1+0.001w)} - (1-\theta)/(G_{skeleton}\rho_w)} \tag{17}$$

Based on formulas (15) and (17),

$$\eta_{mixed\ material} = \rho_{mixed}(1-\theta) \left[\frac{\frac{\theta}{(1-\theta)}(1+\alpha)}{\rho_{filler}} + \frac{1}{G_{skeleton}\rho_w} \right] - 1$$

$$= \left[\frac{\rho_{mixed}(1+\alpha)}{d_s\rho_w(1+0.001w)} - \frac{\rho_{mixed}(1-\theta)\alpha}{G_{skeleton}\rho_w} \right] - 1 \tag{18}$$

Formula (18) is simplified to

$$\eta_{mixed\ material} = \eta(\rho_{mixed}, \theta, \alpha, d_s, \rho_w, w, G_{skeleton}) \qquad (19)$$

Based on formula (19) and an analysis of the situation wherein the microheave filler is completely filled, it was found that mixed material macroscopic expansion is closely related to mixed material compactness $\eta_{mixed\ material}$, filler content θ, filler expansion rate α, mixed material ratio d_s, water compactness ρ_w, microheave filler water content w and skeleton ratio $G_{skeleton}$. Actual frost heave rates are greater than the calculated values.

5.2 Microheave filler partial filling

To further investigate the mixed material frost heave rule, microscopic analysis is required to understand the interactions between pore filler and microheave filler. During filler expansion, mixed material skeleton pores cannot be filled completely. Microheave filler specimens would expand under the side constraint condition. During expansion, the filler would experience plastic deformation and fill skeleton pores, which would result in microheave filler specimen macroscopic elevation. The manifestation of core filler stress is very complex. First, filler grains are not uniformly distributed in all skeleton pores of mixed materials. When stresses on fine aggregates are small, coarse aggregates are not affected, and coarse aggregate skeletons experience no deformation; coarse aggregate and fine aggregate contact surfaces are equivalent to the displacement boundary condition. As the filler expands and fills the remaining part of the skeleton pores, although the fine aggregate stresses are significant, because the expanded filler does not fill all the skeleton pores in the mixed material, the mixed material skeleton grains are not lifted, and the mixed material skeleton does not swell. To summarize, fine aggregates are not completely surrounded by coarse aggregates, pores are interconnected, fine aggregates either expand and deform in large pores or are squeezed to adjacent pores. Therefore, as shown in **Figure 12**, stress state cannot be described via simple mechanical models.

Based on Griffith micro-fracture theory and the minimum energy principle, a calculation formula was deduced via mathematical and mechanical analysis to undertake a quantitative analysis of the effects of rock and soil rheological properties for engineering. Filler was pushed into a cylinder using a porous piston. An analogy from physics was applied, and the filler expansion stress status was compared to the mathematical physics model in **Figure 13**.

Each pore in the microheave filler skeleton was treated as a container, as shown in **Figure 13**. The container top plate was porous, and more holes implied greater skeleton porosity.
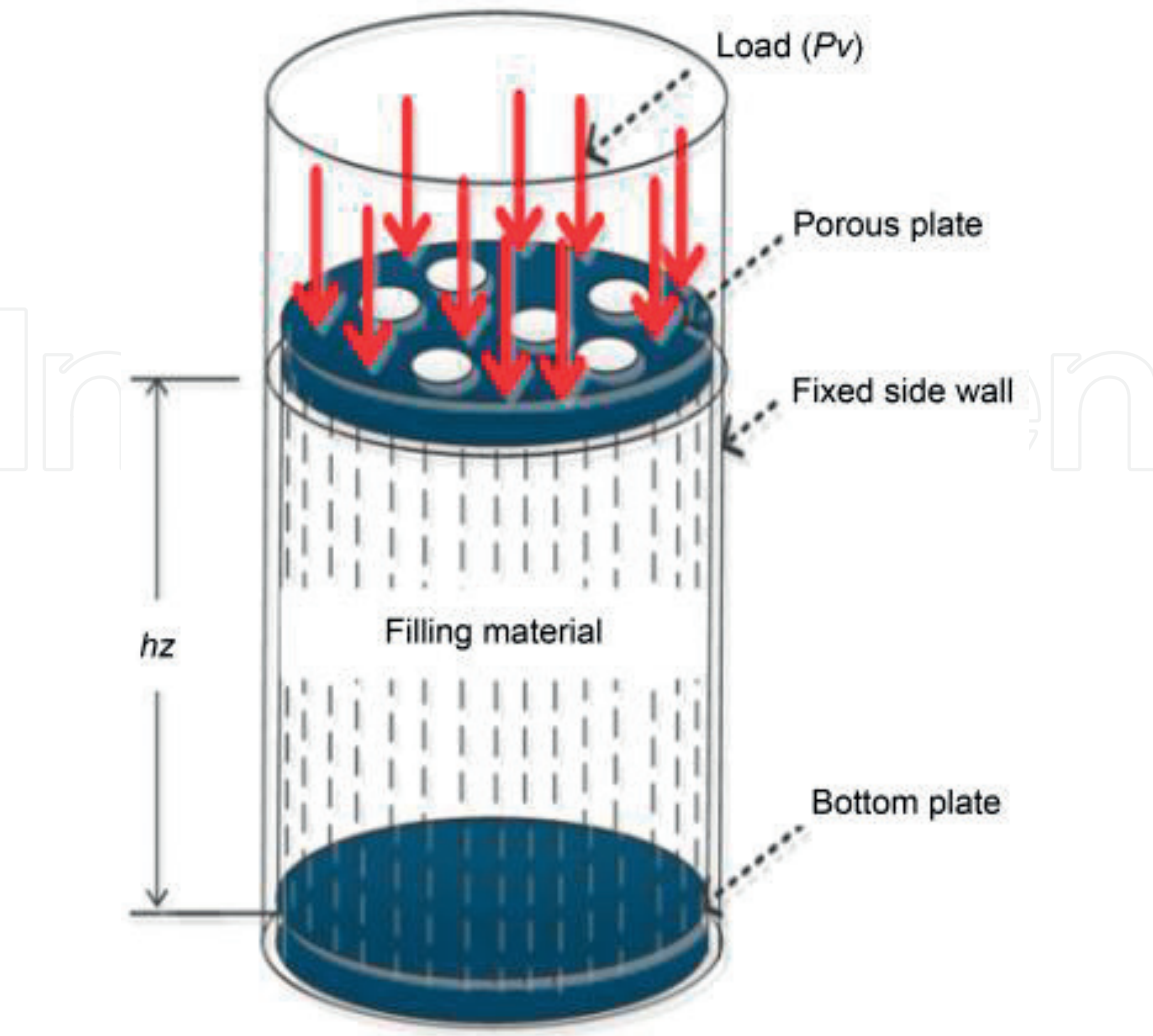
The filling rate reflects the filling degree, which is defined as the ratio of filler volume to skeleton pore volume. Assuming that the mixed material skeleton grain pore filling rate by filler grains is β,

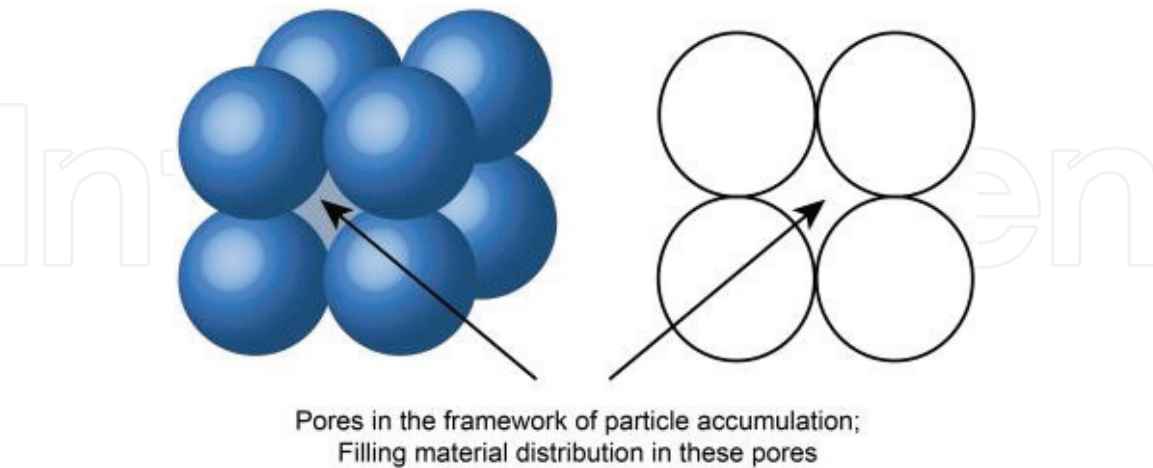$$\beta = \frac{V_{filler}}{V_{skeleton\ pore}} \qquad (20)$$

For an initial filling rate β_0, employing formula (20) yields

$$V_{skeleton\ pore} = \frac{V_{filler}}{\beta} \qquad (21)$$

When filler fills skeleton pores, the mixed material skeleton grain volume does not change during expansion. Mixed material macroscopic volume changes can only be achieved by changing the skeleton pores, as shown by formula (22).

Figure 12.
Skeleton pore filled with filler.

Pores in the framework of particle accumulation;
Filling material distribution in these pores

Figure 13.
Mixed material partial filling.

$$\Delta V_{mixed\ material} = \Delta V_{skeleton\ pore} = \frac{\Delta V_{filler}}{\beta} + \frac{V_{filler}}{\beta} - \frac{V_{filler}}{\beta_0} \qquad (22)$$

When the filler grains expanded, the porous plate moved upward, which increased the macroscopic volume. In addition, some fine grains were extruded via

the top plate pore, and plastic deformation consumed energy, as shown by formula (23).

$$\Delta V_{filler} = \Delta V_{mixed\ material} + \Delta V_{extrude} \tag{23}$$

Based on formulas (22) and (23),

$$\Delta V_{extrude} = \Delta V_{filler} - \frac{\Delta V_{filler}}{\beta} - \frac{V_{filler}}{\beta} + \frac{V_{filler}}{\beta_0} \tag{24}$$

Because filler grains are in a plastic state, their elastic potential energies cannot be increased. Therefore, $\Delta E_{elastic\ potential\ energy}$ = 0.

The mixed material expands by ΔV_{all}, the upper load is N, and the pressure is $p_v = N/S_2$. Assume that the piston area is $S = S_1 + S_2$, where S_1 is the piston area with pores, and S_2 is the piston area without pores. Therefore, the work during expansion is

$$W_{work} = \Delta V_{all}\, p_v \tag{25}$$

Note: $\Delta V_{all}\, p_v$ has units of energy, whereas $\Delta V_{all}\, N$ does not have units of energy.

The extrusion volume is calculated via formula (24). The corresponding soil develops plastic deformation and dissipates energy. Based on a general expression of the plastic strain flow rule under the principle of minimum energy consumption, the plastic deformation energy consumption rate is

$$\psi = \int_v \rho\varphi dv \tag{26}$$

Where $\rho\varphi = \sigma d\varepsilon^p$. The energy dissipation process only occurs when the yield criterion is satisfied. In this paper, plastic energy is the product of the stress friction coefficient and volume strain. That is, $W_{plastic}$ deformation energy consumption is proportional to the soil internal friction coefficient K, soil stress P and soil extrusion volume $\Delta V_{extrude}$. In addition, when β is larger and the area of pores in the porous plate is smaller, it is more difficult to extrude soil, and energy consumption is higher. Therefore, it should be positively correlated with $1/(1-\beta)$. Plastic energy consumption is described by formula (27):

$$W_{plastic\ deformation\ energy\ consumption} = \frac{\chi K P \Delta V_{extrude}}{(1 - \beta)} \tag{27}$$

where K is a dimensionless variable, P is stress, χ is a constant, and $\chi = (1-\beta_0)b$. The solution for P now follows.

A microelement under a porous plate hole to be extruded is in a plastic flow state, and $\sigma_3 = 0$. $\sigma_1 = \sigma_2 > 0$. Based on the Mohr-Coulomb criterion, $\sigma_1 = \sigma_2 = 2c\cos\varphi/(1-\sin\varphi)$.

Therefore,

$$P = \frac{\sigma_1 + \sigma_2 + \sigma_3}{3} = \frac{4}{3}c\,\frac{\cos\varphi}{1 - \sin\varphi} \tag{28}$$

K represents soil friction, and $K = \tan\varphi$.

In this process, the expansion potential energy is

$$\Delta H = \Delta E_{elastic\ potential\ energy} + W_{work} + W_{plastic\ deformation\ energy\ consumption}$$
$$= \Delta V_{mixed\ material} p_v + \chi K P \Delta V_{extrude} \frac{1}{1\text{-}\beta} \tag{29}$$

Based on formulas (22), (24) and (29),

$$\Delta H = \left(\frac{\Delta V_{mixed\ material}}{\beta} + \frac{V_{mixed\ material}}{\beta} - \frac{V_{mixed\ material}}{\beta_0} \right) p_v$$
$$+ \chi K P \left(\Delta V_{mixed\ material} - \frac{\Delta V_{mixed\ material}}{\beta} - \frac{V_{mixed\ material}}{\beta} + \frac{V_{mixed\ material}}{\beta_0} \right) \frac{1}{1\text{-}\beta} \tag{30}$$

According to the principle of minimum energy, the total internal energy of a closed system with steady volume, external parameters and entropy will tend to decrease. When a balance state is reached, the overall internal energy reaches the minimum level. β should result in a minimum ΔH; the range of β is $\beta_0 \leq \beta \leq 1$.

The prerequisite for minimum ΔH is

$$\frac{\partial \Delta H}{\partial \beta} = 0 \tag{31}$$

The filler grain volume expansion rate is $\alpha = \Delta V_{mixed\ material}/V_{mixed\ material}$, and $b = p_v/KP$; then, based on (31),

$$\left(\frac{1}{1-\beta}\chi - b \right) \left(\frac{\alpha}{\beta^2} + \frac{1}{\beta^2} \right) + \chi \left(\alpha - \frac{\alpha}{\beta} - \frac{1}{\beta} + \frac{1}{\beta_0} \right) \frac{1}{(1-\beta)^2} = 0 \tag{32}$$

When $\alpha = 0$, $\beta = \beta_0$. This is substituted into the above formula, yielding $\frac{1}{1-\beta_0}\chi - b = 0$, where $\chi = (1 - \beta_0)b$.

It is easy to prove that when $\alpha \rightarrow +\infty$, $\beta \rightarrow 1^-$. The solution is

$$\left(\alpha\chi - b - \alpha b + \frac{\chi}{\beta_0} \right) \beta^2 + (2ab - 2\chi - 2\alpha\chi + 2b)\beta + (\alpha\chi - b - \alpha b + \chi) = 0 \tag{33}$$

Because the range for β is $\beta_0 \leq \beta \leq 1$, the solution for the single variable quadratic equation (33) is

$$\beta = \frac{A \pm \sqrt{B - C \cdot D}}{E} \tag{34}$$

where

$$A = -(2ab - 2\chi - 2\alpha\chi + 2b),$$
$$B = (2ab - 2\chi - 2\alpha\chi + 2b)^2,$$
$$C = 4\left(\alpha\chi - b - \alpha b + \frac{\chi}{\beta_0} \right), \tag{35}$$
$$D = (\alpha\chi - b - \alpha b + \chi),$$
$$E = 2\left(\alpha\chi - b - \alpha b + \frac{\chi}{\beta_0} \right).$$

Based on formula (34), this is simplified to

$$\beta = \beta(\alpha, b, \chi, \beta_0) \tag{36}$$

where $b = p_v/KP$, $p_v = N/S = N(1+e)$, and $\chi = (1-\beta_0)b$.
Formula (36) is further optimized:

$$\beta = \beta(N, \alpha, C, \varphi, \beta_0) \tag{37}$$

The formula for calculating the partial filling model expansion filling rate shows that the expansion filling rate is closely related to parameters such as the overlying load, filler cohesion, friction angle and initial fill rate.

The relations between these physical variables are

$$e_{skeleton0} = \frac{V_{skeleton\ pore}}{V_{skeleton\ solid}} \tag{38}$$

$$\beta_0 V_{skeleton\ pore} = V_{filler} \tag{39}$$

During expansion,

$$\begin{aligned} e_{skeleton} &= \frac{V_{skeleton\ pore} + \Delta V_{skeleton\ pore}}{V_{skeleton\ solid}} = e_{skeleton0} + \frac{\Delta V_{skeleton\ pore}}{V_{skeleton\ solid}} \\ &= e_0 + \frac{\Delta V_{filler}}{V_{skeleton\ solid}}\left(\frac{\alpha}{\beta} + \frac{1}{\beta} - \frac{1}{\beta_0}\right) \end{aligned} \tag{40}$$

As the skeleton grain pore increases, $\Delta V_{skeleton\ pore} > 0$, $e_{skeleton}$ increases accordingly.

Based on formula (40), if there is only an elevation effect, $\beta_0 = \beta$, the ratio of $\Delta V_{skeleton\ pore}$ versus ΔV_{filler} does not change, and the following always holds:

$$V_{skeleton\ pore} + \Delta V_{skeleton\ pore} = \frac{\left(V_{filler} + \Delta V_{filler}\right)}{\beta_0} \tag{41}$$

Ease of extrusion is directly related to β. In formula (40), if ΔV_{filler} is fixed and only β increases, then $\Delta V_{skeleton\ pore}$ decreases; i.e., small extrusion holes and lower elevations make extrusion difficult.

During filler grain expansion, elevation is calculated via formula (31), and extrusion is calculated via formula (32). The ratio of the two is calculated by substituting β into the two formulae.

5.3 Creation of a microheave filler frost heave model

In an actual project, when the filler is expanding, microheave filler skeleton pores cannot be filled completely. Therefore, the microheave filler frost heave complete filling model should be modified. The microheave filler complete filling theoretical model and partial filling model are combined, and interactions between the filling and elevation effects are considered. The model is created using the principle of minimum energy. For complete filling, the microheave filler frost heave model is described by formula (3). For partial filling, the microheave filler model is described by formula (23).

$$\Delta V_{mixed\ material} = \Delta V_{filler} - \left(\frac{\alpha - \frac{\alpha}{\beta} - \frac{1}{\beta} + \frac{1}{\beta_0}}{\frac{1}{\beta} - 1} \right) \left(V_{skeleton\ pore} - V_{filler} \right) \quad (42)$$

where

$$M = \frac{\alpha - \frac{\alpha}{\beta} - \frac{1}{\beta} + \frac{1}{\beta_0}}{\frac{1}{\beta} - 1} \quad (43)$$

The microheave filler frost heave model is simplified to

$$\Delta V_{mixed\ material} = \Delta V_{filler} - M \left(V_{skeleton\ pore} - V_{filler} \right) \quad (44)$$

The above formula is quantified. Based on formulas (4) and (44),

$$\Delta V_{mixed\ material} = \Delta V_{filler} - M V_{residual\ pore}$$
$$= \frac{m_{filler}}{\rho_{filler}} (M + \alpha) + M \frac{m_{keleton}}{\rho_{keleton}} - M V_{mixed\ material} \quad (45)$$

Based on formulas (3), (45) is rearranged to

$$\Delta V_{混合料} = m_{骨架} \left[\frac{\frac{\theta}{1-\theta} (M + \alpha)}{\rho_{充填料}} + \frac{M}{\rho_{骨架}} \right] - M V_{混合料} \quad (46)$$

Based on formulas (7), (8) and (46),

$$\eta_{mixed\ material} = \frac{\Delta V_{mixed\ material}}{V_{mixed\ material}} = m_{skeleton} \left[\frac{\frac{\theta}{(1-\theta)} (M + \alpha)}{\rho_{filler}} + \frac{M}{\rho_{skeleton}} \right] / V_{mixed\ material} - M \quad (47)$$

Substitution of formulas (11) into (47) yields

$$\eta_{mixed\ material} = m_{skeleton} \left[\frac{\frac{\theta}{(1-\theta)} (M + \alpha)}{\rho_{filler}} + \frac{M}{\rho_{skeleton}} \right] / V_{mixed\ material} - M$$
$$= \rho_{mixed} (1 - \theta) \left[\frac{\frac{\theta}{1-\theta} (M + \alpha)}{\rho_{filler}} + \frac{M}{\rho_{skeleton}} \right] - M \quad (48)$$

Based on the skeleton grain ratio definition, (49) is rearranged as

$$\eta_{mixed\ material} = \rho_{mixed} (1 - \theta) \left[\frac{\frac{\theta}{1-\theta} (M + \alpha)}{\rho_{filler}} + \frac{M}{\rho_{skeleton}} \right] - M$$
$$= \rho_{mixed} (1 - \theta) \left[\frac{\frac{\theta}{1-\theta} (M + \alpha)}{\rho_{filler}} + \frac{M}{G_{skeleton} \rho_w} \right] - M \quad (49)$$

Based on formula (17), the left side is $\Delta V_{all} = \eta_{mixed} hS$. Based on the complete filling model, hS is 1. Rearranging formula (50) yields

$$\eta_{mixed\ material} = \rho_{mixed}(1 - \theta)\left[\frac{\frac{\theta}{1-\theta}(M + \alpha)}{\rho_{filler}} + \frac{M}{\rho_{skeleton}}\right] - M$$

$$= \left[\frac{\rho_{mixed}(M + \alpha)}{d_s\rho_{filler}(1 + 0.01w)} + \frac{\rho_{mixed}(1 - \theta)\alpha}{G_{skeleton}\rho_w}\right] - M$$

(50)

where M is given by formula (43), and β in M is given by formula (35).

To determine β, $b = p_v/KP$ is used, where K represents soil friction, $K = \tan\varphi$, and P is determined using formula (33).

The pressure is $p_v = N/S = N(1 + e)$, and χ is a constant, where $\chi = (1-\beta_0)b$. Formula (51) is simplified to

$$\eta_{mixed\ material} = \eta(N, \varphi, C, \alpha, \beta_0, d_s, \rho_w, w, \rho_{mixed}, \theta, G_{skeleton})$$

(51)

The parameters in relation formula (51) were obtained via the indoor filler frost heave test, and the simple physical and mechanical test was used for the microheave filler.

Based on the microheave filler frost heave model, microheave filler frost heave is closely related to the specimen overlying load, filler plastic deformation friction angle, filler cohesion, filler frost heave rate, mixed material skeleton pore filling rate by the initial filler, mixed material ratio, water density, mixed material water content, mixed material density, filler content and mixed material skeleton ratio.

6. Model verification

Based on the model presented in this paper, the filler frost heave rates for various filler filling rates are shown in **Figure 14**, and the filler frost heave rates for various water contents are shown in **Figure 15**. These results were then compared with the test results presented in this paper.

Figures 14 and **15** show that the model simulation results essentially matched the test results. However, the specimens in the test and simulation differed. A silt filler frost heave rate test under an overlying load of N_1 = 60 kPa was performed. Other parameters, including the model parameters, are listed in **Table 5**.

The filler frost heave rate in the lab is $\eta_{mixed\ material}$ = 0.123 mm/ 150 mm = 0.082%.

The simulation showed that when the water content was 9%, the frost heave rate was approximately 0.22%.

A comparison of the calculated and experimental filler frost heave rates showed a difference of only 0.06%, which indicates that the microheave filler frost heave computational model derived in this paper is viable for frost heave rate calculations.

7. Conclusions

To solve problems of seasonal permafrost region subgrade filler microheave in China, the effects of influencing factors, such as the filler content, natural water holding capacity, filler grading, permeability coefficient and water supply
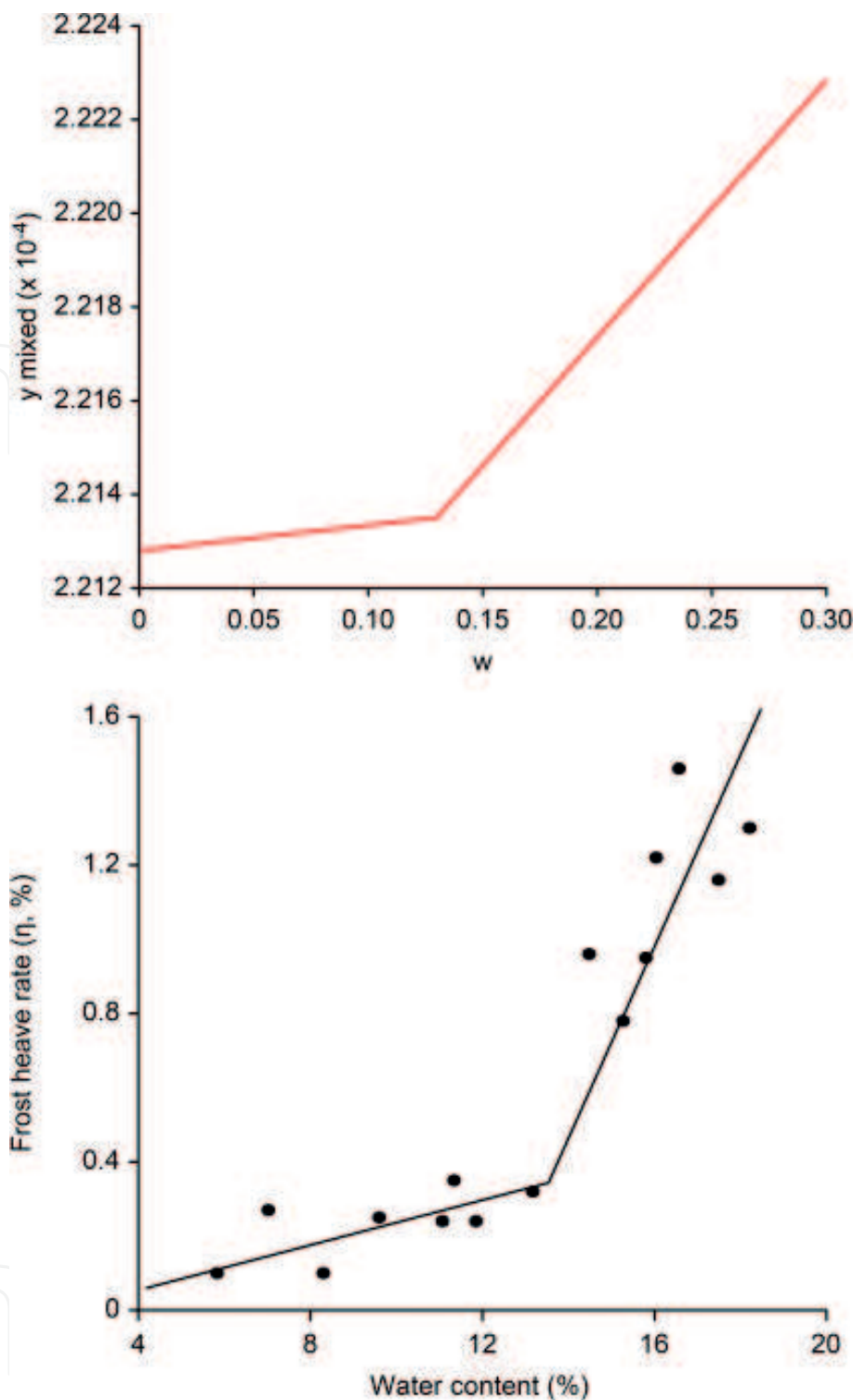
Figure 14.
Frost heave rate versus filler content.

condition, on the subgrade frost heave rate with or without external constraints (overlying train loads) were investigated via an indoor frost heave characteristics test. On that basis, models for complete and partial filling microheave filler frost heave were created. The validity of the theoretical microheave filler frost heave rate forecast model was demonstrated via indoor testing. The detailed conclusions are as follows.

1. The filler grading frost heave test showed that when the gravel or finer aggregate was reduced, the filler frost heave rate decreased gradually; however, even for very low levels of fine grain content at low temperatures,
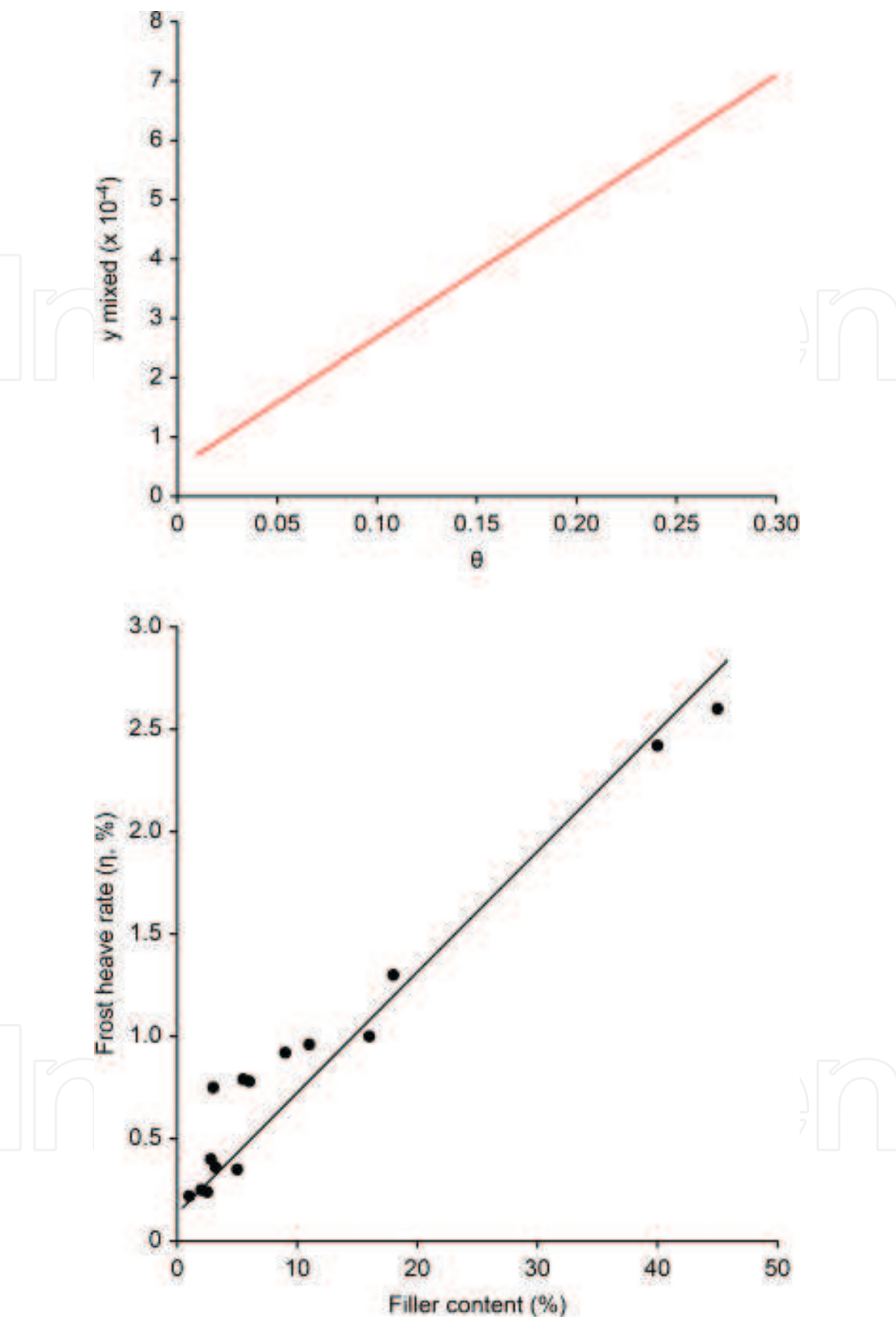
Figure 15.
Variations in frost heave rate with water content.

w_p	C_1	φ	ρ	e	β_0	w	α
9	6	30°	2.1	0.3	0.178	9%	0.22%

Table 5.
Model parameters.

the soil still produced a certain level of frost heave. The filler overlying load test showed that an overlying pressure produced a certain level of suppression effects on filler frost heave.

2. Microheave filler frost heave increased with filler frost heave; however, when the filler fill rate was under 0.25, as the filler content increased, the changes in filler frost heave were insignificant. This means that at this condition, filler frost heave filled pores, no filler macroscopic frost heave occurred, and soil was insensitive to frost heave. For filler filling rates exceeds 0.25, as the filling rate increased, the filler frost heave rate increased significantly, and the soil was sensitive to frost heave.

3. A microheave filler frost heave model, $\eta_{mixed\ material} = \eta(N, \varphi, C, \alpha, \beta_0, d_s, \rho_w, w, \rho_{mixed}, \theta, G_{skeleton})$, which considers the overlying load, filler plastic deformation friction angle, filler cohesion, filler frost heave rate, mixed material skeleton pore filling rate by the initial filler, mixed material ratio, water density, mixed material water content, mixed material density, filler content and mixed material skeleton ratio, was created. The applicability of the microheave filler frost heave model was verified via testing.

Acknowledgements

Notes

α	filler expansion rate
β	mixed material skeleton grain pore filling rate by filler grains
β_0	initial filling rate by filler grains
d_s	mixed material ratio
$\Delta E_{elastic\ potential\ energy}$	D-value of elastic potential energy
$G_{skeleton}$	skeleton grain ratio
Δh	overall specimen frost heave in mm
ΔH	expansion potential energy
H_f	frozen depth (excluding frost heave) in mm
η	microheave filler frost heave rate
$\eta_{mixed\ material}$	mixed material frost heave rate
η_{filler}	filler compactness
θ	filler content
K	soil internal friction coefficient, $K = \tan\varphi$
M_1	skeleton grain mass for a unit specimen volume
M_2	filler mass for a unit specimen volume
m_{filler}	quality of filler
$m_{mixed\ material}$	quality of mixed material
$m_{skeleton}$	quality of skeleton
N	upper load
ρ_{filler}	density of filler
$\rho_{mixed\ material}$	density of mixed material
$\rho_{skeleton}$	density of skeleton

ρ_w	water compactness
P	soil stress
p_v	pressure
γ_1	skeleton grain dry density for the corresponding soil sample compactness
γ_2	filler dry density for the corresponding soil sample compactness
s	specimen's filler volume fill rate
S	piston area
S_1	piston area with pores
S_2	piston area without pores
V_1	filler skeleton grain volume fraction
V_2	filler volume fraction
$V_{mixed\ material}$	mixed material grain volume fraction
ΔV_{all}	mixed material expands
$\Delta V_{extrude}$	soil extrusion volume
ΔV_{filler}	D-value of filler volume fraction
$\Delta V_{mixed\ material}$	D-value of mixed material grain volume fraction
$\Delta V_{residual\ pore}$	D-value of residual pore volume fraction
$\Delta V_{skeleton\ pore}$	D-value of skeleton pore volume fraction
ω	difference between the filler initial water content
ω_0	filler optimal water content
ω_p	filler plastic limit water content
ω_v	filler volumetric water content
$W_{plastic\ deformation\ energy\ consumption}$	work during plastic deformation energy consumption
W_{work}	work during expansion
w	microheave filler water content
ψ	plastic deformation energy consumption rate
χ	a constant

Author details

Ye Yangsheng, Du Xiaoyan, Zhang Qianli and Chai Jinfei*
China Academy of Railway Sciences, Railway Engineering Research Institute, Beijing, China

*Address all correspondence to: chaijinfei@gmail.com

IntechOpen

References

[1] Ye YS, Cai DG, Yan HY, Yao JP, Zhang QL, Cheng AJ. The mechanism analysis of micro frost heave coarse-grained filling material in the high-speed railway. Japanese Geotechnical Society Special Publication. 2016;**2**(47): 1660-1663

[2] Chen X, Liu J, Liu H. Frost action of soil and foundation engineering. Beijing: Science Press; 2011 (in Chinese)

[3] Askar Z, Zhanbolat S. Experimental investigations of freezing soils at ground conditions of Astana, Kazakhstan. Sciences in Cold and Arid Regions. 2015; **7**(4):0399-0406

[4] Konrad J-M. Freezing-induced water migration in compacted base-course materials. Canadian Geotechnical Journal. 2008;**45**(7):895-909

[5] Konrad JM, Lemieux N. Influence of fines on frost heave characteristics of a well-graded base-course material. Canadian Geotechnical Journal. 2005; **42**(2):515-527

[6] Bilodeau J-P, Dore G, Pierre P. Gradation influence on frost susceptibility of base granular materials. International Journal of Pavement Engineering. 2008;**9**(6):397-411

[7] Uthus L, Hermansson Å, Horvli I, Hoff I. A study on the influence of water and fines on the deformation properties and frost heave of unbound aggregates. In: International Conference on Cold Regions Engineering, pp. 1-13

[8] Wang T, Yue Z, Sun T. Influence of fines content on the anti-frost properties of coarse-grained soil. Sciences in Cold and Arid Regions. 2015;**7**(4):0407-0413

[9] Bilodeau JP, Doré G, Poupart J. Permanent deformation of various unbound aggregates submitted to seasonal frost conditions. Cold Regions Engineering. 2012:155-164

[10] Guo Y, Yang Y, Zeng L. Study on frost heaving characteristics of subgrade soil of lanzhou-xinjiang railway. Subgrade Engineering. 2010;**2**:149-151

[11] Sheng DC, Zhang S, Niu F, Cheng G. A potential new frost heave mechanism in high-speed railway embankments. Géotechnique. 2014;**64**(2):144-154

[12] Abdalla B, Fan C, Mckinnon C, Gaffard V, Audibert-Hayet A, Coche E, et al. Extended porosity rate function for frost heave. In: ASME 2014 33rd International Conference on Ocean, Offshore and Arctic Engineering, ASME. San Francisco, CA; 2010. V010T007A046

[13] Zhang Y, Michalowski RL. Multiphysical modeling and numerical simulation of frost heave and thaw settlement. In: Geo-congress 2014 Technical papers@ sgeo-characterization and modeling for sustainability, ASCE, Atlanta, GA; 2014. pp. 2735-2744

[14] Bronfenbrener L. The modelling of the freezing process in fine-grained porous media: Application to the frost heave estimation. Cold Regions Science and Technology. 2009;**56**(2):120-134

[15] Yin C. Study on Seasonal Permafrost Region Subgrade soil Frost Heave Characteristics and Evaluation Index System. Northeast Forestry University; 2014

[16] Wang Z, Zhang Q, Ye Y. In-depth study on the classification of filling for railway subgrade. China Railway Science. 2012;**33**(2):13-20

[17] Li A, Niu YH, Niu F, Liu H. Research status of frost heaving

properties and controlling measures of coarse grained soil. Journal of Glaciology and Geocryology. 2015;**37**(1):202-210

[18] Du X. Research on Filler Frost Heave and Coarse Grain Skeleton Interaction-Based Micro Heave Filler Frost Heave Mechanism. Beijing: China Academy of Railway Sciences; 2015

[19] Tian Y, Liu J, Peng L. Experimental study on frost action of fine-grained soils under dynamic and static loads. Chinese Journal of Geotechnical Engineering. 2010;**32**(12):1882-1888

[20] Zhao H, Yan H, Zhang Q, et al. Study on frost-heave performances of filler consisting of coarse grained soils for subgrade bed in seasonal frozen region. Railway Engineering. 2014;**7**: 92-94